

## Accepted Manuscript

Synthesis of hydrolysis-resistant pyridoxal 5'-phosphate analogs and their biochemical and X-ray crystallographic characterization with the pyridoxal phosphatase chronophin

Gunnar Knobloch, Nauras Jabari, Sven Stadlbauer, Hermann Schindelin, Maja Köhn, Antje Gohla

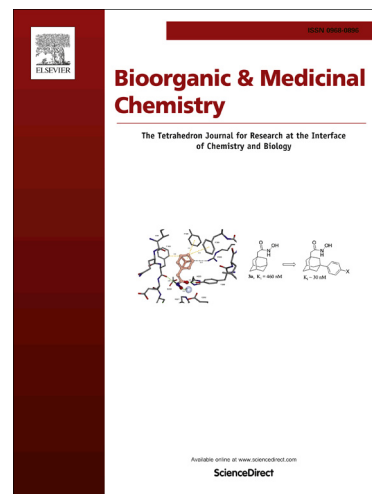
PII: S0968-0896(15)00153-4  
DOI: <http://dx.doi.org/10.1016/j.bmc.2015.02.049>  
Reference: BMC 12112

To appear in: *Bioorganic & Medicinal Chemistry*

Received Date: 16 January 2015  
Revised Date: 24 February 2015  
Accepted Date: 25 February 2015

Please cite this article as: Knobloch, G., Jabari, N., Stadlbauer, S., Schindelin, H., Köhn, M., Gohla, A., Synthesis of hydrolysis-resistant pyridoxal 5'-phosphate analogs and their biochemical and X-ray crystallographic characterization with the pyridoxal phosphatase chronophin, *Bioorganic & Medicinal Chemistry* (2015), doi: <http://dx.doi.org/10.1016/j.bmc.2015.02.049>

This is a PDF file of an unedited manuscript that has been accepted for publication. As a service to our customers we are providing this early version of the manuscript. The manuscript will undergo copyediting, typesetting, and review of the resulting proof before it is published in its final form. Please note that during the production process errors may be discovered which could affect the content, and all legal disclaimers that apply to the journal pertain.



**Synthesis of hydrolysis-resistant pyridoxal 5'-phosphate analogs and their biochemical and X-ray crystallographic characterization with the pyridoxal phosphatase chronophin**

Gunnar Knobloch<sup>1,2,4</sup>, Nauras Jabari<sup>1,3,4</sup>, Sven Stadlbauer<sup>3</sup>, Hermann Schindelin<sup>2</sup>, Maja Köhn<sup>3,\*</sup>, Antje Gohla<sup>1,2,\*</sup>

<sup>1</sup>Institute of Pharmacology and Toxicology, University of Würzburg, Versbacher Strasse 9, D-97078 Würzburg, Germany

<sup>2</sup>Rudolf Virchow Center for Experimental Biomedicine, University of Würzburg, Josef-Schneider-Strasse 2, D-97080 Würzburg, Germany

<sup>3</sup>EMBL Heidelberg, Genome Biology Unit, Meyerhofstrasse 1, D-69117 Heidelberg, Germany

<sup>4</sup>Equal contributions

\*Corresponding authors. Tel.: +49 931 3180099 (A.G.), +49 6221 3878544 (M.K.).

Email addresses: antje.gohla@virchow.uni-wuerzburg.de (A.G.), koehn@embl.de (M.K.)

**ABSTRACT**

A set of phosphonic acid derivatives (**1-4**) of pyridoxal 5'-phosphate (PLP) was synthesized and characterized biochemically using purified murine pyridoxal phosphatase (PDXP), also known as chronophin. The most promising compound **1** displayed primarily competitive PDXP inhibitory activity with an  $IC_{50}$  value of 79  $\mu$ M, which was in the range of the  $K_m$  of the physiological substrate PLP. We also report the X-ray crystal structure of PDXP bound to compound **3**, which we solved to 2.75 Å resolution (PDB code 5AES). The co-crystal structure proves that compound **3** binds in the same orientation as PLP, and confirms the mode of inhibition to be competitive. Thus, we identify compound **1** as a PDXP phosphatase inhibitor. Our results suggest a strategy to design new, potent and selective PDXP inhibitors, which may be useful to increase the sensitivity of tumor cells to treatment with cytotoxic agents.

**Keywords:**

Cancer therapy

Chronophin

Haloacid dehalogenase-type phosphatase

Pyridoxal 5'-phosphate phosphatase

Non-hydrolyzable pyridoxal 5'-phosphate analogs

## 1. Introduction

Phosphatases of the haloacid dehalogenase (HAD)-type superfamily are emerging as enzymes that are linked to cancer risk, cancer pathogenesis and sensitivity of cancer cells to treatment with cytotoxic agents or  $\gamma$ -irradiation[1-6]. Despite their potential importance as therapeutic target molecules, very few inhibitors of mammalian HAD phosphatases have been reported so far[7-12]. Structurally, HAD phosphatases are typified by a modified Rossmann fold that positions the catalytic core residues. The first aspartate in the conserved DxDx(V/T) HAD phosphatase signature motif serves as the nucleophile and phosphoryl group acceptor that forms a phosphoaspartate intermediate during catalysis. This aspartate also coordinates the catalytically essential  $Mg^{2+}$ -ion[13]. HAD phosphatases are additionally equipped with structurally highly diversified modules, the cap domains, which contribute to catalytic efficiency and phosphatase specificity[13, 14].

Pyridoxal phosphatase (PDXP, also known as chronophin[15]) is a HAD phosphatase dedicated to the metabolism of pyridoxal 5'-phosphate (PLP; Fig. 1) with a  $K_m$  of 1.5  $\mu M$  or 36  $\mu M$  for the human or murine enzymes, respectively[14, 16]. PLP is the biologically active form of vitamin B6 that functions as a cofactor in the catalysis of more than 140 different enzymatic reactions, including trans- and deaminations, decarboxylations, racemizations, aldol cleavage reactions, eliminations and substitutions at  $\beta$ - and  $\gamma$ -atoms of amino acid side chains[17]. In mammals, enzymes using PLP as a prosthetic group are involved in the synthesis of neurotransmitters, amino acid metabolism, glycogen breakdown, heme biosynthesis and lipid metabolism[18].

A recent cohort study has demonstrated that increased metabolism and disposal of vitamin B6 is associated with a higher risk of developing malignant neoplasms, in particular lung cancer[19]. Moreover, elevated circulating vitamin B6 levels are inversely correlated with the risk of developing non-small cell lung cancer (NSCLC)[20]. Importantly, low expression levels of the PLP-generating pyridoxal kinase (PDXK) can serve as a biomarker for poorer disease outcome in NSCLC patients[21, 22]. The same study showed that a membrane-permeable PLP precursor sensitizes lung cancer cell lines to lethal responses induced by various types of physical stressors and chemotherapeutics, and that PDXK is required for optimal cytotoxic effects[21]. Consistent with these findings, depletion of PDXP was observed to sensitize cancer cells to death, and cisplatin-resistant cells exhibited a decreased PDXK/PDXP ratio, either due to decreased PDXK or to increased PDXP protein levels[21].

Furthermore, overexpression of PDXP transcripts has been observed in clinical NSCLC specimens[23]. Although the mechanistic basis of each of these effects remains to be fully understood, an increase in cellular PLP levels may sensitize cancer cells to cytotoxic insults by targeting PLP-dependent enzymes that influence stress-relevant metabolic circuitries[17]. Together, these data suggest that PLP elevation in cancer cells may be beneficial as an adjuvant pharmacological strategy in cancer therapy.

Attempts to increase PLP levels in cancer cells by inhibiting the PLP-catabolizing PDXP have not yet been described. However, this approach may be valuable in cancers with PDXK deficiency or PDXP overexpression, which is the case in a subset of NSCLC patients[21, 23]. As a first step towards this aim, we have synthesized hydrolysis-resistant PLP analogs (Fig. 1, compounds **1-4**) to target the active site of PDXP, and have characterized their inhibitory potential using purified PDXP. Furthermore, we have solved the first X-ray crystal structure of PDXP bound to one of these substrate analogs. Our results lay the groundwork for structure-based drug design of active site-directed, potent and specific PDXP inhibitors.

## 2. Results and discussion

### 2.1. Chemistry

We designed the hydrolysis-resistant PLP analogs by replacing the 5'-phosphate group of PLP with a phosphonate. The 4'-position of the PLP pyridine ring was either substituted with an aldehyde (compound **1**, Fig. 1), as in PLP, or with an alcohol (compound **3**, Fig. 1), as in the PLP precursor pyridoxine phosphate (PNP). Furthermore, a double bond was introduced at the 5'-position of the pyridine ring in order to study the impact of the resulting structural rigidity of the phosphonate residue on the inhibition potency of compounds **1** and **3** (compounds **2** and **4**, Fig. 1).

The synthesis of the four compounds was based on published procedures[24, 25]. In the first step, commercially available pyridoxine was dimethyl acetal-protected on the 3'- and 4'-hydroxy groups (Scheme 1). Oxidation of the alcohol on the 5'-position furnished aldehyde **6**, which was then subjected to a Wittig-reaction with tetraethyl methylenediphosphonate to yield phosphonate **7**[24]. Deprotection of the hydroxyl groups led to phosphonate **8**, and the four reaction steps proceeded with good to excellent yields. The final compound **4** was obtained by cleavage of the ethyl esters of the phosphonate group of compound **8** using trimethylsilyl (TMS)-bromide[26]. Aldehyde **2** was synthesized by oxidation of the 4'-alcohol of compound

**8** and subsequent TMS-Br mediated deprotection. To obtain final compounds **1** and **3**, the double bond of compound **8** was reduced to furnish **9**, which was again deprotected using TMS-Br to yield alcohol **3**. Oxidation of compound **9** and subsequent TMS-Br mediated deprotection provided aldehyde **1**.

## 2.2. PDXP inhibition

The hydrolysis-resistant PLP analogs (compounds **1-4**) were characterized biochemically in dose-response and steady state kinetic assays using recombinantly expressed and highly purified murine PDXP. Dose-response assays employing PDXP (100 nM) and its physiological substrate PLP (20  $\mu$ M) showed that the half-maximal inhibitory concentration ( $IC_{50}$ ) of compounds **1** or **2** (containing an aldehyde in the 4'-position) towards PDXP was reached at  $79 \pm 1.2 \mu$ M or  $246 \pm 1.1 \mu$ M, respectively. Thus, the presence of a C-C double bond in the 5'-position in compound **2** increased the  $IC_{50}$  by approximately 3-fold compared to compound **1**. Compounds **3** and **4** (containing an alcohol at the 4'-position) had ~5–16-fold higher  $IC_{50}$  values of around 1.3 mM (Fig. 2).

The kinetic constants derived from steady state kinetic measurements of PDXP-catalyzed PLP dephosphorylation in the presence of compounds **1-4** demonstrated that compounds **1** and **2** increased the  $K_m$  up to ~6-fold at the highest tested compound concentrations (2 mM). In addition, the calculated  $v_{max}$  and the  $k_{cat}$  values were reduced ~2-fold under these conditions. As a result, the catalytic efficiency ( $k_{cat}/K_m$ ) of PDXP was reduced to ~10% in the presence of 2 mM compound **1** compared to buffer control conditions. Compounds **3** and **4** increased the  $K_m$  up to ~3–5-fold, but did not markedly affect  $v_{max}$  and  $k_{cat}$ . The catalytic constants are summarized in Table 1. These data confirm that compounds **1-4** indeed act primarily as competitive PDXP inhibitors, although the  $v_{max}$  and  $k_{cat}$  changes observed in the presence of compounds **1** and **2** may point to an additional inhibitory mechanism.

The results presented above indicate that the presence of an aldehyde group as compared to an alcohol group at the 4'-position of the substrate analogs may result in a greater binding affinity to PDXP. This is in line with a previous study reporting that an increase in electronegativity at the 4'-position lowers the  $K_m$  value of B6 vitamers when assayed with human PDXP ( $K_m$  pyridoxamine phosphate (PMP), 34  $\mu$ M;  $K_m$  pyridoxine phosphate (PNP), 5.19  $\mu$ M;  $K_m$  pyridoxal phosphate (PLP) 1.47  $\mu$ M[16]). The crystal structures of human PDXP in complex with PLP (PDB codes 2P69 and 2CFT) show that PLP is coordinated by an

extensive binding network in the active site, taking advantage of every electronegative atom on the molecule. In addition, the PLP pyridine ring interacts with the imidazole ring of His182 in the PDXP substrate specificity loop by  $\pi$ -electron stacking (distance, 3.3–3.8 Å; Fig. 3)[14]. The structures do not reveal any strong binding interactions between the 4'-aldehyde and its surrounding residues. Nevertheless, the 4'-aldehyde has the potential to build weak hydrogen bonds with several adjacent residues through multiple water bridges, and it can additionally form a weak hydrogen bond to Asn60 (mean distance, 3.4 Å; Fig. 3). Based on this information, we hypothesize that the binding affinity and inhibitory efficacy of PLP analogs might be further increased by substituents that bring the 4'-aldehyde moiety –or another proton accepting functional group at this position– closer to Asn60. Additionally, the presence of a more electronegative moiety in the 4'-position may induce a greater pulling effect on the  $\pi$ -electrons of the pyridine ring, thus facilitating  $\pi$ -electron-stacking with His182.

### 2.3. X-ray crystal structure of inhibitor 3 in complex with PDXP

For detailed structural information on the interactions of compounds 1-4 with murine PDXP, we attempted to co-crystallize them with PDXP. Although several PDXP crystals were obtained in the presence of all compounds, only a structure of PDXP in complex with compound 3 contained electron density representing the entire substrate analog. The PDXP·compound 3-complex crystallized in space group I23, and the structure was solved by molecular replacement using the previously solved structure of murine PDXP/chronophin (PDB code 4BX3). The structure was subsequently refined to 2.75 Å resolution with an  $R_{\text{cryst}}$  of 19.0% and an  $R_{\text{free}}$  of 24.7% (PDB code 5AES). The data collection and refinement statistics are summarized in Table 2.

Figure 4 shows an overview of the PDXP·compound 3-complex and a detailed view of the inhibitor bound to the active site of PDXP. As previously reported for murine PDXP, which exists as a homo-dimer in solution, PDXP also crystallized as a homodimer in complex with compound 3 [14]. The overall structure of murine PDXP remains unaltered by ligand binding, as indicated by a root mean square (r.m.s.) deviation of 0.26 Å when the structure was aligned with the previously solved structure of murine apo-PDXP (PDB code 4BX3). The coordination of compound 3 within the catalytic pocket of murine PDXP is similar to the coordination of PLP bound to human PDXP (PDB codes 2P69 and 2CFT). The residues that are closest to the alcohol group in the 4'-position of compound 3 are Asp27 (mean distance,

3.75 Å) and Asn60 (mean distance, 4.75 Å). These distances are too far for hydrogen bonding, but could allow van der Waals interactions. Nevertheless, since the mean distance between the 4'-aldehyde group of PLP and Asn60 in human PDXP (PDB code 2CFT) spans only 3.5 Å and results in the formation of a weak hydrogen bond, replacing the alcohol group in the 4'-position of compound **3** with an aldehyde function should likewise result in hydrogen bonding interactions with Asn60. Asn60 is the terminal amino acid in the HAD consensus motif II (<sup>56</sup>FVSNN<sup>60</sup> in human and mouse PDXP); the strictly conserved Ser58 in this motif helps to orient the substrate for the nucleophilic attack and to stabilize the phosphoaspartate intermediate that is formed during catalysis[13] (Fig. 5).

The PDXP·compound **3** structure will facilitate the rational development of inhibitory compounds with higher efficacy and specificity for PDXP. PLP analogs containing a 4'-aldehyde group can be expected to affect the activities of all PLP-dependent enzymes. This is because the use of PLP as a prosthetic group involves the formation of a covalent Schiff-base with the 4'-aldehyde group of PLP and the ε-amino group of a lysine side chain in the active site of the respective enzyme[17]. The introduction of electronegative functional groups other than an aldehyde at the 4'-position of hydrolysis-resistant substrate analogs is expected to increase the affinity of the compounds for PDXP[16], and at the same time to prevent binding to PLP-dependent enzymes. It has been reported that PLP substituted with a phenylalanine at the 4'-position [N-(5'-phospho-4'-pyridoxyl)phenylalanine] is a better PDXP substrate than PNP[27]. Consistent with our structural data, this finding suggests that PDXP tolerates bulky substituents at the 4'-position, which could be exploited to improve the specificity of second generation PDXP inhibitors (Fig. 5). The same study also showed that the chemical modification of arginines with phenylglyoxal led to PDXP inactivation, which was prevented in the presence of PLP, thus suggesting that at least one arginine residue is involved in PLP coordination[27]. Indeed, the X-ray crystal structures of both human and murine PDXP reveal three arginines in the entrance of the active site (see Figs. 3 and 5; PDB codes 2P69, 2CFT and 4BKM). This positively charged region (the 'arginine mouth') may be accessed by replacing the PLP 4'-position with negatively charged substituents of sufficient length.

Other modifications that may increase the affinity of active site-directed PDXP inhibitors described in the present study involve the insertion of a difluoromethylphosphonate group at the 5'-position to form hydrogen bonds with Ser58 and Asn60 backbone atoms of the PDXP catalytic domain. Finally, replacements of the 2'-methyl group with other hydrophobic

substituents may increase hydrophobic interactions with Tyr146 (Tyr150) of the capping domain in murine (human) PDXP (Fig. 5).

### 3. Conclusions

The elevation of intracellular PLP levels by means of inhibiting the activity of the pyridoxal phosphatase PDXP/chronophin is a novel concept to increase the sensitivity of cancer cells to cytotoxic agents. We show here that PDXP inhibition is feasible by targeting its active site using PLP-based antimetabolites. The synthesis of non-hydrolyzable PLP analogs, which were prepared previously and assayed for their biological activity against tyrosine decarboxylase apo-enzyme and aspartate aminotransferase[24], proceeded successfully following published procedures[24-26]. Aldehyde **1** was the most potent inhibitor of PDXP-catalyzed PLP hydrolysis, with an  $IC_{50}$  of  $79 \pm 1.2 \mu\text{M}$ , which is in the range of the  $K_m$  of the physiological substrate PLP ( $K_m = 42 \mu\text{M}$  PLP for murine PDXP in the current study). Thus, the 4'-aldehyde group in the PLP analogs appears to be an important structural element for the recognition by PDXP. The presence of compound **1** in kinetic measurements of PDXP-mediated PLP hydrolysis led to an increase of the  $K_m$ , but did not markedly change  $v_{\text{max}}$ , showing that compound **1** is primarily a competitive inhibitor of PDXP. While this compound was not entirely visible in the crystal structure in complex with PDXP, the complex of PDXP bound to another hydrolysis-resistant substrate analog (alcohol **3**) was solved by X-ray crystallography (2.75 Å, PDB code 5AES). The co-crystal structure proves that compound **3** binds in the same orientation as the natural substrate PLP does, and confirms the mode of inhibition to be competitive. In summary, we identified compound **1** as the first inhibitor of PDXP phosphatase activity. The PDXP-compound **3** structure can now be used to design new inhibitors of PDXP that are less PLP-like, in order to potentially achieve selectivity over other PLP-binding proteins.

## 4. Experimental protocols

### 4.1. Chemistry

Anhydrous solvents and all reagents were purchased from Sigma-Aldrich. All reactions involving air- or moisture-sensitive compounds were performed under argon atmosphere using dried glassware and syringes techniques to transfer solutions. Nuclear magnetic resonance ( $^1\text{H}$  NMR,  $^{31}\text{P}$  NMR,  $^{13}\text{C}$  NMR) spectra were recorded using a 400 MHz Bruker Avance DPX. Chemical shifts ( $\delta$ ) are reported in parts per million (ppm) and the coupling

constants (J) are expressed in Hertz (Hz). Splitting patterns are designated as follows: s, singlet; d, doublet; sept, septet; t, triplet; q, quadruplet; m, multiplet; br s, broad singlet; br m, broad multiplet; dd, double of double. The assignment of exchangeable protons (NH) was confirmed by the addition of D<sub>2</sub>O. Analytical thin-layer chromatography (TLC) was carried out on Merck silica gel F-254 plates. HPLC analysis and purifications were carried out on a Shimadzu High Performance Liquid Chromatograph/Mass Spectrometer LCMS-2010EV with a UV/Vis photodiode array detector SPD-M20A Prominence. The analytical column was a Macherey Nagel C18 EC 250/4.0 NUCLEODUR 100-5 C18 ec for gradients of 10–100% CH<sub>3</sub>CN in water and a Macherey Nagel EC 250/4.6 NUCLEODUR C18 Pyramid for gradients starting from 0%. For preparative separations a Macherey Nagel C18 VP 250/21 NUCLEODUR 100-C5 C18 ec column was used. For purity analysis and mass spectrometry an Agilent Technologies UPLC 1290 Infinity system coupled with a 6120 Quadrupole mass spectrometer was used.

### 3,4-*O*-isopropylidene pyridoxine **5**

To a mixture of pyridoxine (3.5 g, 20.7 mmol) in CH<sub>2</sub>Cl<sub>2</sub> (70 mL) dimethoxypropane (21.1 mL, 172 mmol) and 96% H<sub>2</sub>SO<sub>4</sub> (1.25 mL, 23.5 mmol) were added under argon atmosphere. The mixture was refluxed at 45 °C for 6 h, resulting in a deep brownish/red color. The solution was then diluted with CH<sub>2</sub>Cl<sub>2</sub>, washed with sodium bicarbonate, and extracted with CH<sub>2</sub>Cl<sub>2</sub>. The combined organic fractions were dried over sodium sulfate, and concentrated in vacuo. The crude compound was re-dissolved in a mixture of Et<sub>2</sub>O/pentane (2:1) and refluxed at 40 °C for 30 min. During this time, the desired product began crystallizing. The solution was then tempered to room temperature and kept at –25 °C for 30 h. The precipitate was collected *via* suction filtration and washed with cold (–25 °C) pentane to afford **5** as a fluffy, white, crystalline solid (3.72 g, 86%): mp 106–107 °C; <sup>1</sup>H NMR (400 MHz, CDCl<sub>3</sub>) δ 1.55 (s, 6H), 2.39 (s, 3H), 2.79 (s-broad, 1H), 4.56 (s, 2H), 4.94 (s, 2H), 7.86 (s, 1H). <sup>13</sup>C NMR (100 MHz, CDCl<sub>3</sub>) δ 18.1, 24.7, 58.6, 60.0, 99.8, 126.1, 129.7, 138.4, 146.1, 147.5. HPLC-MS (10–100% CH<sub>3</sub>CN in H<sub>2</sub>O with 0.1% TFA; flow rate 1.5 mL/min): t<sub>R</sub> = 5.8 min; m/z: 210.0 [M+H]<sup>+</sup>.

### 3,4-*O*-isopropylidene pyridoxal **6**

MnO<sub>2</sub> (27.6 g, 317 mmol) was added to a solution of **5** (3.70 g, 17.7 mmol) in CH<sub>2</sub>Cl<sub>2</sub> (36 mL) and the mixture was stirred vigorously for 2 h at room temperature. Then the reaction mixture was filtered through a short silica column to remove the MnO<sub>2</sub> and the product was

eluted with  $\text{CH}_2\text{Cl}_2$ . Subsequent evaporation yielded **6** as a pale yellow syrup (1.91 g, 51%). Further purification by column chromatography (100% EtOAc) afforded a clear and viscous liquid that formed solid white plates at room temperature or in a freezer, mp 57–59 °C;  $^1\text{H}$  NMR (400 MHz,  $\text{CDCl}_3$ )  $\delta$  1.56 (s, 6H), 2.51 (s, 3H), 5.18 (s, 2H), 8.47 (s, 1H), 10.04 (2, 1H).  $^{13}\text{C}$  NMR (100 MHz,  $\text{CDCl}_3$ )  $\delta$  18.8, 24.7, 60.2, 100.5, 126.3, 144.8, 147.8, 153.5, 191.4. HPLC-MS (10–100%  $\text{CH}_3\text{CN}$  in  $\text{H}_2\text{O}$  with 0.1% TFA; flow rate 1.5 mL/min):  $t_{\text{R}}$  = 7.1 min;  $m/z$ : 208.1  $[\text{M}+\text{H}]^+$ , 415.2  $[\text{M}_2+\text{H}]^+$ .

#### Diethyl 2-(3,4-*O*-isopropylidene-2-methyl-5-pyridyl)ethenylphosphonate **7**

A solution of  $\text{CH}_2[\text{PO}(\text{OEt})_2]_2$  (4.73 mL, 19.0 mmol) in cyclohexane (15 mL) was added to a suspension of NaH (399 mg, 60% in mineral oil, 9.98 mmol) in cyclohexane (15 mL) at room temperature, resulting in vigorous production of gas. After the reaction mixture became clear, a solution of **6** (1.88 g, 9.07 mmol) in 15 mL of cyclohexane, was added dropwise at room temperature. After approximately 60% of the aldehyde had been added, a thick, gummy precipitate formed at reaction scales over 1 g of **6**. The resulting mixture was stirred for 1 h, then diluted with a mixture of  $\text{CHCl}_3/\text{H}_2\text{O}$  (2:1), and extracted three times with  $\text{CH}_2\text{Cl}_2$ . The combined organic fractions were concentrated to provide a slightly viscous amber liquid, which was subjected to column chromatography (EtOAc/Cyclohexane (1:1)) to afford **7** as an amorphous white solid (2.94 g, 95%).  $^1\text{H}$  NMR (400 MHz,  $\text{CDCl}_3$ )  $\delta$  1.36 (t, 6H), 1.56 (s, 6H), 2.17 (s, 4H), 2.44 (s, 3H), 4.14 (m, 4H), 4.91 (s, 2H), 6.23 (t, 1H), 7.33 (dd, 1H), 8.23 (s, 1H).  $^{31}\text{P}$  NMR (162 MHz,  $\text{CDCl}_3$ )  $\delta$  17.7 (s).

#### Diethyl 2-(3-hydroxy-4-hydroxymethyl-2-methyl-5-pyridyl)ethenylphosphonate **8**

**7** (3.61 g, 12.0 mmol) was refluxed in a 10% solution of  $\text{HCO}_2\text{H}$  in  $\text{H}_2\text{O}$  (20 mL) for 1 h, resulting in a clear, yellow solution. Although starting material was left, it was crucial to stop the reaction after 1 h in order to prevent formation of side-products. Upon completion, the water solution was concentrated and the resulting residue purified *via* column chromatography ( $\text{CH}_2\text{Cl}_2/\text{MeOH}$  (9:1)), which afforded **8** as pale yellow plates (2.3 g, 72%). Mp 96.5–97.5 °C;  $^1\text{H}$  NMR (400 MHz,  $\text{CDCl}_3$ )  $\delta$  1.34 (t, 6H), 2.52 (s, 3H), 4.09 (m, 4H), 5.10 (s, 2H), 6.18 (t, 1H), 7.46 (dd, 1H), 8.09 (s, 1H).  $^{13}\text{C}$  NMR (100 MHz,  $\text{CDCl}_3$ )  $\delta$  14.6, 16.4 ( $^3J_{\text{CP}} = 5$  Hz), 60.7, 63.0 ( $^2J_{\text{CP}} = 5$  Hz), 100.0, 123.0, 124.7, 127.9, 130.8, 138.4, 143.5.  $^{31}\text{P}$  NMR (162 MHz,  $\text{CDCl}_3$ )  $\delta$  17.3 (s). UPLC-MS (5–100%  $\text{CH}_3\text{CN}$  in  $\text{H}_2\text{O}$  with 0.1% TFA; flow rate 1.5 mL/min):  $t_{\text{R}}$  = 1.13 min;  $m/z$  = 302.1  $[\text{M}+\text{H}]^+$ .

**2-(3-hydroxy-4-hydroxymethyl-2-methyl-5-pyridyl)ethenylphosphonic acid 4**

Under argon atmosphere bromotrimethylsilane (262  $\mu\text{L}$ , 19.9 mmol) was added dropwise to a solution of **8** (100 mg, 0.33 mmol) in  $\text{CH}_2\text{Cl}_2$  (2 mL) and the resulting mixture was stirred for 6 h at room temperature. Then bromotrimethylsilane (87  $\mu\text{L}$ , 0.66 mmol) was added again and the mixture was stirred overnight at room temperature. The reaction was quenched by addition of water and the mixture was extracted with water. The combined aqueous phases were lyophilized and the product was obtained in quantitative yield. No further purification was required [26]. Solubility in water was low when re-solubilizing the compound. Due to this low solubility,  $^{13}\text{C}$  chemical shifts were obtained indirectly from HSQC experiments for those C-atoms bearing protons. Mp  $>210$   $^\circ\text{C}$  (dec);  $^1\text{H}$  NMR (400 MHz,  $\text{D}_2\text{O}$ )  $\delta$  2.62 (s, 3H), 4.99 (s, 2H), 6.53 (t, 2H), 7.41 (dd, 1H), 8.29 (s, 1H).  $^{13}\text{C}$  NMR (100 MHz,  $\text{D}_2\text{O}$ )  $\delta$  14.0, 56.3, 128.7, 129.4, 133.4.  $^{31}\text{P}$  NMR (162 MHz,  $\text{CDCl}_3$ )  $\delta$  10.5 (s). UPLC-MS (5–100%  $\text{CH}_3\text{CN}$  in  $\text{H}_2\text{O}$  with 0.1% TFA; flow rate 1.5 mL/min):  $t_{\text{R}}$  = 0.19 min;  $m/z$  = 246.0  $[\text{M}+\text{H}]^+$ .

**Diethyl 2-(3-hydroxy-4-hydroxymethyl-2-methyl-5-pyridyl)ethylphosphonic acid 9**

To a solution of **8** (1.46 g, 4.85 mmol) in ethanol (40 mL), Pd on charcoal (163 mg, ca. 10% Pd, 0.15 mmol) was added and the resulting suspension hydrogenated at 1 atm of  $\text{H}_2$  at room temperature for 1 h. The black suspension was filtered and the solution was concentrated in vacuo, followed by recrystallization in EtOAc/Et $_2$ O (1:1). **9** was obtained as a greyish-white solid (0.78 g, 53%): mp 107.5–109  $^\circ\text{C}$ ;  $^1\text{H}$  NMR (400 MHz,  $\text{CDCl}_3$ )  $\delta$  1.29 (t, 6H), 1.88 (m, 2H), 2.43 (s, 3H), 2.79 (m, 2H), 4.03 (m, 4H), 4.86 (s, 2H), 7.77 (s, 1H).  $^{13}\text{C}$  NMR (100 MHz,  $\text{CDCl}_3$ )  $\delta$  14.5, 16.4, 16.5, 22.7, 25.3, 25.9 (d,  $^1J_{\text{CP}}$  = 110 Hz), 59.6, 62.36, 62.42, 66.7, 130.6, 135.0, 135.1, 139.3, 141.6, 148.1, 154.3.  $^{31}\text{P}$  NMR (162 MHz,  $\text{CDCl}_3$ )  $\delta$  30.2 (s). UPLC-MS (5–100%  $\text{CH}_3\text{CN}$  in  $\text{H}_2\text{O}$  with 0.1% TFA; flow rate 1.5 mL/min):  $t_{\text{R}}$  = 1.12 min;  $m/z$  = 304.1  $[\text{M}+\text{H}]^+$ .

**Diethyl 2-(4-formyl-3-hydroxy-2-methyl-5-pyridyl)ethylphosphonate 10**

$\text{MnO}_2$  (1.21 g, 13.9 mmol) was added to a solution of **9** (0.30 g, 0.99 mmol) dissolved in  $\text{CHCl}_3$  (24 mL) and the resulting suspension was stirred vigorously for 1.5 h at room temperature. Then the suspension was filtered through a short silica column to remove the  $\text{MnO}_2$  and the product was eluted with  $\text{CHCl}_3$ . Subsequent evaporation yielded **10** as a highly viscous deep golden-yellow syrup (280 mg, 94%).  $^1\text{H}$  NMR (400 MHz,  $\text{D}_2\text{O}$ )  $\delta$  1.34 (m, 6H), 2.07 (m, 1 H), 2.35 (m, 1H), 2.73 (s, 1H), 2.85 (s, 1H), 3.39 (m, 3 H), 4.13 (m, 4H), 8.30 (s, 1H), 10.58 (s, 1H).  $^{13}\text{C}$  NMR (100 MHz,  $\text{D}_2\text{O}$ )  $\delta$  15.0, 16.4, 18.4, 21.7, 26.8, 62.4, 62.6,

113.0, 122.4, 132.7, 137.8, 147.5, 154.7, 194.5.  $^{31}\text{P}$  NMR (162 MHz,  $\text{D}_2\text{O}$ )  $\delta = 32.4$ . HPLC-MS (10–50%  $\text{CH}_3\text{CN}$  in  $\text{H}_2\text{O}$  with 0.1% TFA; flow rate 1.5 mL/min):  $t_{\text{R}} = 7.6$  min;  $m/z$ : 302.0  $[\text{M}+\text{H}]^+$ .

### **2-(3-hydroxy-4-hydroxymethyl-2-methyl-5-pyridyl)ethylphosphonic acid 3**

Under argon atmosphere bromotrimethylsilane (522  $\mu\text{L}$ , 3.96 mmol) was added dropwise to a solution of **9** (200 mg, 0.66 mmol) in  $\text{CH}_2\text{Cl}_2$  (4 mL) and the resulting mixture was stirred for 6 h at room temperature. Then bromotrimethylsilane (174  $\mu\text{L}$ , 1.32 mmol) was added again and the mixture was stirred overnight at room temperature. The reaction was quenched by addition of  $\text{H}_2\text{O}$  and the product extracted into the aqueous layer, followed by lyophilization. Although after bromotrimethylsilane-treatment no further purification was required due to the side products being either volatile or remaining in the organic layer [26], we purified the resulting residue with preparative HPLC (0–30%  $\text{CH}_3\text{CN}$  in  $\text{H}_2\text{O}$ , flow rate 5 ml/min) to ensure its purity, which led to the loss of a large amount of the compound due to solubility issues. Fractions containing the product were combined, the solvent evaporated and the aqueous solution lyophilized, affording **3** as white solid powder (11.8 mg, 7.2%).  $^1\text{H}$  NMR (400 MHz,  $\text{D}_2\text{O}$ )  $\delta$  1.84 (m, 2H), 2.56 (s, 3H), 2.94 (m, 2H), 4.97 (s, 2H), 8.02 (s, 1H).  $^{13}\text{C}$  NMR (100 MHz,  $\text{D}_2\text{O}$ )  $\delta$  14.1, 23.7, 27.6, 28.9, 56.8, 131.1, 138.2, 140.9, 152.8.  $^{31}\text{P}$  NMR (162 MHz,  $\text{D}_2\text{O}$ )  $\delta$  22.6 (s). HPLC-MS (NUCLEODUR C18 Pyramid column, 0–30%  $\text{CH}_3\text{CN}$  in  $\text{H}_2\text{O}$  with 0.1% TFA; flow rate 1.5 mL/min):  $t_{\text{R}} = 2.2$  min;  $m/z$ : 248.1  $[\text{M}+\text{H}]^+$ , 495.2  $[\text{M}_2+\text{H}]^+$ .

### **2-(4-formyl-3-hydroxy-2-methyl-5-pyridyl)ethylphosphonic acid 1**

Under argon atmosphere bromotrimethylsilane (612  $\mu\text{L}$ , 4.64 mmol) was added dropwise to a solution of **10** (233 mg, 0.77 mmol) in  $\text{CH}_2\text{Cl}_2$  (4.5 mL) and the mixture was stirred for 6 h at room temperature. Then bromotrimethylsilane (78  $\mu\text{L}$ , 0.59 mmol) was added again and the mixture was stirred overnight at room temperature. The reaction was quenched by addition of  $\text{H}_2\text{O}$  and the product extracted into the aqueous layer followed by lyophilization, and the product was obtained in quantitative yield. No further purification was required [26].

Solubility issues were encountered when trying to re-dissolve the compound, and it was not possible to obtain sufficient NMR spectra. HPLC-MS (NUCLEODUR C18 Pyramid column, 0–50%  $\text{CH}_3\text{CN}$  in  $\text{H}_2\text{O}$  with 0.1% TFA; flow rate 1.5 ml/min):  $t_{\text{R}} = 2.1$  min;  $m/z$ : 246.0  $[\text{M}+\text{H}]^+$ .

**Diethyl 2-(4-formyl-3-hydroxy-2-methyl-5-pyridyl)ethenylphosphonic acid 11**

MnO<sub>2</sub> (1.24 g, 14.3 mmol) was added to a solution of **8** (310 mg, 1.03 mmol) in CHCl<sub>3</sub> (25 mL) and the resulting mixture was stirred vigorously for 1.5 h at room temperature, filtered through a short silica column to remove the MnO<sub>2</sub>, and the product was eluted with CHCl<sub>3</sub>. Subsequent evaporation yielded **11** as a light greenish-yellow syrup (0.27 g, 88%). <sup>1</sup>H NMR (400 MHz, CDCl<sub>3</sub>) δ 1.36 (t, 6H), 2.55 (s, 3H), 4.16 (m, 4H), 6.31 (t, 1H), 7.95 (dd, 1H), 8.24 (s, 1H), 10.42 (s, 1H). <sup>13</sup>C NMR (100 MHz, CDCl<sub>3</sub>) δ 16.4, 19.0, 62.3, 118.8, 122.1, 124.0, 129.0, 137.8, 139.8, 153.1, 195.4. <sup>31</sup>P NMR (162 MHz, CDCl<sub>3</sub>) δ 16.0 (s).

**2-(4-formyl-3-hydroxy-2-methyl-5-pyridyl)ethenylphosphonic acid 2**

Under argon atmosphere bromotrimethylsilane (524 μL, 3.97 mmol) was added dropwise to a solution of **11** (198 mg, 0.66 mmol) in CH<sub>2</sub>Cl<sub>2</sub> (4 mL) and the resulting mixture was stirred for 6 h at room temperature. Then bromotrimethylsilane (175 μL, 1.33 mmol) was added again and the mixture was stirred overnight at room temperature. The reaction was quenched by addition of H<sub>2</sub>O and the product was extracted into the aqueous layer followed by lyophilization, and the product was obtained in quantitative yield. No further purification was required [26]. <sup>13</sup>C chemical shifts were obtained indirectly from HSQC experiments for those C-atoms bearing protons. However, the signal for the aldehyde group was not visible. Mp >150 °C (dec); <sup>1</sup>H NMR (400 MHz, MeOD<sub>4</sub>) δ 2.57 (s, 3H), 6.53 (dd, 1H, <sup>3</sup>J<sub>HH</sub> = 16 Hz, <sup>2</sup>J<sub>HP</sub> = 16 Hz), 7.40 (dd, 1H, <sup>3</sup>J<sub>HH</sub> = 20 Hz, <sup>3</sup>J<sub>HP</sub> = 16 Hz), 8.22 (s, 1H), 10.52 (s, 1H). <sup>13</sup>C NMR (100 MHz, MeOD<sub>4</sub>) δ 138.7, 134.7, 126.0, 16.1. <sup>31</sup>P NMR (162 MHz, MeOD<sub>4</sub>) δ 9.6 (s). UPLC-MS (5–100% CH<sub>3</sub>CN in H<sub>2</sub>O with 0.1% TFA; flow rate 1.5 mL/min): t<sub>R</sub> = 0.19 min; m/z = 262.1 [M+H<sub>2</sub>O+H]<sup>+</sup>.

**4.2. Protein expression and purification**

Murine PDXP/chronophin cDNA was reverse-transcribed from adult mouse brain tissue. Total RNA was isolated using TRIzol (Invitrogen) according to the manufacturer's instructions, and cDNA was obtained with the High Fidelity RNA PCR Kit (Takara) and oligo dT primers. The PCR product was subcloned into the bacterial expression vector pETM11 (EMBL) to create N-terminally His<sub>6</sub>-tagged chronophin for *in vitro* studies. His<sub>6</sub>-tagged PDXP was transformed into BL21(DE3) cells (Stratagene), and expressed for 18 h at 20°C after induction with 0.5 mM isopropyl β-D-1-thiogalactopyranoside (IPTG). Cells were harvested at 8,000 × g for 10 min and lysed in 100 mM triethanolamine (TEA), 500 mM NaCl, 20 mM imidazole, 5 mM MgCl<sub>2</sub>; pH 7.4, in the presence of protease inhibitors (EDTA-

free protease inhibitor tablets, Roche) and 150 U/ml DNase I (Applichem) using a cell disruptor (Microfluidizer Processor M-110 P, Microfluidics). Cell debris was removed by centrifugation for 30 min at  $30,000 \times g$ . For purification, cleared supernatants were loaded on a HisTrap HP column operated on an ÄKTA liquid chromatography system (GE Healthcare) in binding buffer (50 mM TEA, 500 mM NaCl, 20 mM imidazole, 5 mM  $MgCl_2$ ; pH 7.4), and His<sub>6</sub>-tagged proteins were eluted using a linear gradient up to 50% elution buffer (50 mM TEA, 250 mM NaCl, 500 mM imidazole, 5 mM  $MgCl_2$ ; pH 7.4). Fractions containing His<sub>6</sub>-tagged PDXP were pooled, and the His<sub>6</sub>-tag was cleaved with tobacco etch virus (TEV)-protease for 2 days at 4°C. Subsequently, cleaved protein was separated from uncleaved protein and from the His<sub>6</sub>-tagged TEV-protease on a HisTrap HP column. Untagged PDXP was further purified on a HiLoad 16/60 Superdex 200 pg size exclusion chromatography column (GE Healthcare) in buffer A [50 mM TEA, 250 mM NaCl, 5 mM  $MgCl_2$ , 5% (v/v) glycerol; pH 7.4].

#### 4.3. *In vitro* PDXP phosphatase inhibitor assays

Pyridoxal 5'-phosphate (PLP) dephosphorylation assays were conducted in the absence and presence of substrate analogs in 96- or 384-well microtiter plates (for kinetic or dose-response assays, respectively). One hundred nM of PDXP per well were pre-incubated for 10 min at 22°C in buffer A supplemented with 0.001% (v/v) Triton X-100, followed by 4 min of incubation with the respective compound (dissolved in 50 mM TEA, 250 mM NaCl, 5 mM  $MgCl_2$ ; pH 7.4). The reactions were started by the addition of PLP. The final PLP concentration was set to 20  $\mu$ M in dose-response assays, or ranged between 0–500  $\mu$ M in kinetic assays. The final volume of each reaction was 50  $\mu$ L for kinetic assays, and 25  $\mu$ L for dose-response assays. Kinetic measurements were stopped after 2 min, and dose-response assays were stopped after 5 min by the addition of 50 or 100  $\mu$ L Biomol Green, respectively (Enzo Life Sciences). Color was allowed to develop for 15–20 min before the absorbance of the resulting phosphomolybdate complex was read at 620 nm on an Envision 2104 multilabel microplate reader (Perkin Elmer). Free phosphate release was quantified using phosphate standard curves, and  $v_{max}$  and  $K_m$  values were calculated using GraphPad Prism (GraphPad Software Inc.), version 6. The lines were fitted by nonlinear regression using the least squares fitting method. For dose-response assays,  $\log_{inhibitor}$  versus response was calculated for a Hill slope of -1.

#### 4.4. Crystallization and data collection

PDXP was concentrated to 8–10 mg/mL (as determined by absorption at 280 nm using a calculated molar extinction coefficient of  $18,450 \text{ M}^{-1} \cdot \text{cm}^{-1}$ ) in 10 mM TEA, 100 mM NaCl, 1 mM  $\text{MgCl}_2$  using 10 kDa MWCO centrifugal filter devices (Amicon Ultra-15, Millipore). The crystals were grown at 20°C using the hanging-drop vapor-diffusion method, by mixing equal volumes of protein solution with reservoir solution. The protein was crystallized in 0.1 M imidazole, 0.2 M NaCl and 1 M sodium tartrate, supplemented with 5 mM compound **3**. The cubic crystals appeared within hours after setting up the crystallization experiment. All crystals were cryoprotected for flash-cooling in liquid nitrogen by soaking in mother liquor containing 30% (v/v) glycerol. PDXP diffraction data were collected on an R-axis HTC imaging plate detector mounted on a Micromax HF-007 rotating anode X-ray generator. Data were processed using iMosflm[28] and scaled with Scala from the CCP4 program suite[29]. The structure was solved by molecular replacement with the program Phaser [30] using the previously solved murine PDXP/chronophin structure (PDB entry 4BX3) as a search model. Ligand restraints for the refinement of compound **3** were generated using the electronic Ligand Builder and Optimization Workbench (eLBOW[31]) and the Restraints Editor Especially Ligands (REEL) of the Phenix program suite[32, 33]. The PDXP structure in complex with compound **3** was refined at 2.75 Å resolution with Phenix[34], incorporating torsion angle non-crystallographic symmetry (ncs) restraints. Data collection and refinement statistics are summarized in Table 2. The figures were generated with PyMOL (The PyMol Molecular Graphics System, version 1.5.0.4, Schrödinger, LLC). The X-ray crystal structure of murine PDXP/chronophin bound to compound **3** has been deposited in the Protein Data Bank under accession code 5AES.

## FIGURE LEGENDS

**Figure 1.** PLP and the non-hydrolyzable analogs used in this study.

**Scheme 1.** Synthesis of compounds **1-4**. Reagents and conditions: a) dimethoxypropane, H<sub>2</sub>SO<sub>4</sub>, CH<sub>2</sub>Cl<sub>2</sub> reflux, 6h, argon; b) MnO<sub>2</sub>, CH<sub>2</sub>Cl<sub>2</sub>, r.t., 2h; c) CH<sub>2</sub>[PO(OEt)<sub>2</sub>]<sub>2</sub>, NaH, cyclohexane, r.t., 2h; d) 10% HCO<sub>2</sub>H in H<sub>2</sub>O, reflux, 1h; e) 10% Pd/C, H<sub>2</sub>, ethanol, r.t., 1h; f) MnO<sub>2</sub>, CHCl<sub>3</sub>, r.t., 1.5h; g) TMS-Br in CH<sub>2</sub>Cl<sub>2</sub>, r.t., 6h, argon, then again TMS-Br overnight (see the experimental protocols for the low yield of compound **3**). r.t. = room temperature.

**Figure 2.** Dose-response curves of PDXP-mediated PLP dephosphorylation in the presence of compounds **1-4** (**A**) or compound **1** (**B**). The results represent mean values ± S.E. of three independently performed experiments conducted with three independently purified batches of protein. Controls were conducted in the absence of compounds. Control values of each experiment in **A** were normalized to the mean of *n*=3 measurements. Errors bars not seen are hidden within the symbols.

**Figure 3.** Coordination of PLP in the active site of human PDXP (PDB code 2CFT). Water molecules are represented as red spheres.

**Figure 4.** Structure of murine PDXP in complex with compound **3** (PDB code 5AES). (**A**) One protomer of the homodimeric PDXP is shown as a cartoon representation (rainbow color), the other protomer is depicted as a surface representation (gray). Compound **3** is shown in green and the cofactor Mg<sup>2+</sup> as a magenta sphere. A detailed structure of the bound inhibitor and adjacent residues of the active site is shown in the boxed area. An F<sub>o</sub>-F<sub>c</sub> omit electron density map of the inhibitor is contoured at an r.m.s. deviation of 3 in red and is superimposed with the refined model. (**B**) Structural comparison of murine PDXP in complex with compound **3** (rainbow color) and human PDXP in complex with PLP (gray, PDB code 2CFT). The boxed area shows the overall structure and positioning of the ligands (green, compound **3**; gray, PLP).

**Figure 5.** Structure of compound **3** with adjacent residues of murine PDXP that might be targeted to increase the specificity and affinity of the PDXP inhibitors described in this study.

Sites for possible modifications are indicated by color-coded dashed lines. For details, see 2.3.

Water molecules are omitted for clarity.

ACCEPTED MANUSCRIPT

## TABLES

**Table 1.** Steady-state kinetic constants of PDXP-catalyzed PLP hydrolysis in the presence of compounds **1-4**.

		Inhibitor concentration [mM]				
		control	0.1	0.5	1.0	2.0
Cmp <b>1</b>	$K_m$ [ $\mu\text{M}$ ]	39 $\pm$ 1.7	72 $\pm$ 2.7	170 $\pm$ 9.6	197 $\pm$ 14.4	246 $\pm$ 38.7
	$v_{max}$ [nmol/min/mg]	3,687 $\pm$ 44	3,588 $\pm$ 45	3,278 $\pm$ 79	2,620 $\pm$ 86	2,131 $\pm$ 161
	$k_{cat}$ [ $\text{s}^{-1}$ ]	2.0 $\pm$ 0.02	1.9 $\pm$ 0.02	1.7 $\pm$ 0.04	1.4 $\pm$ 0.05	1.1 $\pm$ 0.09
	$k_{cat}/K_m$ [ $\text{s}^{-1}\cdot\text{M}^{-1}$ ]	$5.0 \times 10^4$	$2.7 \times 10^4$	$1.0 \times 10^4$	$0.7 \times 10^4$	$0.5 \times 10^4$
Cmp <b>2</b>	$K_m$ [ $\mu\text{M}$ ]	38 $\pm$ 1.7	78 $\pm$ 3.6	170 $\pm$ 13.3	248 $\pm$ 36.6	224 $\pm$ 70.0
	$v_{max}$ [nmol/min/mg]	3,839 $\pm$ 49	3,577 $\pm$ 55	2,986 $\pm$ 99	2,301 $\pm$ 163	1,644 $\pm$ 238
	$k_{cat}$ [ $\text{s}^{-1}$ ]	2.0 $\pm$ 0.03	1.9 $\pm$ 0.03	1.6 $\pm$ 0.05	1.2 $\pm$ 0.09	0.9 $\pm$ 0.13
	$k_{cat}/K_m$ [ $\text{s}^{-1}\cdot\text{M}^{-1}$ ]	$5.4 \times 10^4$	$2.4 \times 10^4$	$0.9 \times 10^4$	$0.5 \times 10^4$	$0.4 \times 10^4$
Cmp <b>3</b>	$K_m$ [ $\mu\text{M}$ ]	49 $\pm$ 3.0	59 $\pm$ 8.1	83 $\pm$ 4.6	98 $\pm$ 11.0	136 $\pm$ 10.9
	$v_{max}$ [nmol/min/mg]	3,843 $\pm$ 70	3,739 $\pm$ 159	3,680 $\pm$ 71	3,440 $\pm$ 140	3,148 $\pm$ 101
	$k_{cat}$ [ $\text{s}^{-1}$ ]	2.0 $\pm$ 0.04	2.0 $\pm$ 0.08	2.0 $\pm$ 0.04	1.8 $\pm$ 0.07	1.7 $\pm$ 0.05
	$k_{cat}/K_m$ [ $\text{s}^{-1}\cdot\text{M}^{-1}$ ]	$4.2 \times 10^4$	$3.3 \times 10^4$	$2.4 \times 10^4$	$1.9 \times 10^4$	$1.2 \times 10^4$
Cmp <b>4</b>	$K_m$ [ $\mu\text{M}$ ]	40 $\pm$ 2.7	44 $\pm$ 5.6	77 $\pm$ 10.7	112 $\pm$ 18.5	181 $\pm$ 28.0
	$v_{max}$ [nmol/min/mg]	3,535 $\pm$ 66	3,304 $\pm$ 121	3,226 $\pm$ 151	3,148 $\pm$ 195	3,074 $\pm$ 206
	$k_{cat}$ [ $\text{s}^{-1}$ ]	1.9 $\pm$ 0.04	1.8 $\pm$ 0.06	1.7 $\pm$ 0.08	1.7 $\pm$ 0.10	1.6 $\pm$ 0.11
	$k_{cat}/K_m$ [ $\text{s}^{-1}\cdot\text{M}^{-1}$ ]	$4.6 \times 10^4$	$4.0 \times 10^4$	$2.2 \times 10^4$	$1.5 \times 10^4$	$0.9 \times 10^4$

The data are mean values  $\pm$  S.E. of three independent experiments performed with three independently purified batches of proteins. Cmp, compound.  $K_m$ , Michaelis-Menten constant;  $v_{max}$ , maximum enzyme velocity;  $k_{cat}$ , turnover number;  $k_{cat}/K_m$ , specificity constant. The  $k_{cat}$  values were calculated from the maximum enzyme velocities using a molecular mass of 31.828 kDa for PDXP. Control measurements were conducted in buffer without inhibitor.

**Table 2.** Data collection and refinement statistics of the PDXP·compound **3** structure.

Data collection		Refinement	
Wavelength (Å)	1.5418	Wilson B-factor (Å <sup>2</sup> )	67.0
Space group	I23	Average B-factor (Å <sup>2</sup> )	50.8
Unit cell parameters		macromolecules	50.9
a = b = c (Å)	166.81	solvent	35.5
α = β = γ (°)	90	R <sub>cryst</sub> <sup>e</sup>	0.1895 (0.2628)
Resolution range (Å) <sup>a</sup>	32.71–2.75 (2.90–2.75)	R <sub>free</sub> <sup>e</sup>	0.2466 (0.2902)
R <sub>sym</sub> <sup>b</sup>	0.098 (0.952)	Number of non H-atoms	4486
R <sub>p.i.m.</sub> <sup>c</sup>	0.039 (0.380)	macromolecules	4403
<I/σI> <sup>d</sup>	13.0 (1.9)	ligands	40
Completeness (%)	100 (100)	water	43
Multiplicity	7.3 (7.2)	Rms deviations in	
Total reflections	147756	bond lengths (Å)	0.006
Unique reflections	20219 (2925)	bond angles (°)	0.932
		planar groups (Å)	0.004
		dihedral angles (°)	14.18
		Coordinate error (Å) <sup>f</sup>	0.34
		Ramachandran statistics <sup>g</sup>	
		favored (%)	98.44
		allowed (%)	0.87
		outliers (%)	0.69
		MolProbity clashscore <sup>h</sup>	8.02

<sup>a</sup> Numbers in parentheses refer to the respective highest resolution data shell in the data set.

<sup>b</sup>  $R_{\text{sym}} = \frac{\sum_{\text{hkl}} \sum_i |I_i - \langle I \rangle|}{\sum_{\text{hkl}} \sum_i I_i}$ , where  $I_i$  is the  $i^{\text{th}}$  measurement, and  $\langle I \rangle$  is the weighted mean of all measurements of  $I$ .

<sup>c</sup>  $R_{\text{p.i.m.}} = \frac{\sum_{\text{hkl}} (1/(n-1))^{1/2} \sum_i |I_i - \langle I \rangle|}{\sum_{\text{hkl}} \sum_i I_i}$ , where  $n$  is the multiplicity of the observed reflection.

<sup>d</sup>  $\langle I/\sigma I \rangle$ : Indicates the average of the intensity divided by its standard deviation.

<sup>e</sup>  $R_{\text{cryst}} = \frac{\sum |F_o - F_c|}{\sum |F_o|}$  where  $F_o$  and  $F_c$  are the observed and calculated structure factor amplitudes.  $R_{\text{free}}$ , same as  $R_{\text{cryst}}$  for 5% of the data randomly omitted from the refinement.

<sup>f</sup> Estimated coordinate error based on  $R_{\text{free}}$ .

<sup>g</sup> Ramachandran statistics indicate the fraction of residues in the favored, allowed and disallowed regions of the Ramachandran diagram, as defined by MolProbity[35].

<sup>h</sup> number of serious clashes per 1000 atoms (Reference: see <sup>g</sup>).

**ACKNOWLEDGEMENTS**

This work was supported by the Deutsche Forschungsgemeinschaft (SFB688 to A.G., and FZ82 to A.G. and H.S.). M.K. thanks the Deutsche Forschungsgemeinschaft for support within the Emmy Noether program. G.K. was supported by a career development fellowship from the Graduate School of Life Sciences at the University of Würzburg, and N.J. was jointly supported by the SFB688 and EMBL.

ACCEPTED MANUSCRIPT

## REFERENCES

- [1] R. Possemato, K.M. Marks, Y.D. Shaul, M.E. Pacold, D. Kim, K. Birsoy, S. Sethumadhavan, H.K. Woo, H.G. Jang, A.K. Jha, W.W. Chen, F.G. Barrett, N. Stransky, Z.Y. Tsun, G.S. Cowley, J. Barretina, N.Y. Kalaany, P.P. Hsu, K. Ottina, A.M. Chan, B. Yuan, L.A. Garraway, D.E. Root, M. Mino-Kenudson, E.F. Brachtel, E.M. Driggers, D.M. Sabatini, Functional genomics reveal that the serine synthesis pathway is essential in breast cancer, *Nature*, 476 (2011) 346-350.
- [2] A. Seifried, J. Schultz, A. Gohla, Human HAD phosphatases: structure, mechanism, and roles in health and disease, *The FEBS journal*, 280 (2013) 549-571.
- [3] I.M. Wilson, E.A. Vucic, K.S. Enfield, K.L. Thu, Y.A. Zhang, R. Chari, W.W. Lockwood, N. Radulovich, D.T. Starczynowski, J.P. Banath, M. Zhang, A. Pusic, M. Fuller, K.M. Lonergan, D. Rowbotham, J. Yee, J.C. English, T.P. Buys, S.A. Selamat, I.A. Laird-Offringa, P. Liu, M. Anderson, M. You, M.S. Tsao, C.J. Brown, K.L. Bennewith, C.E. MacAulay, A. Karsan, A.F. Gazdar, S. Lam, W.L. Lam, EYA4 is inactivated biallelically at a high frequency in sporadic lung cancer and is associated with familial lung cancer risk, *Oncogene*, 33 (2014) 4464-4473.
- [4] K. Wu, Z. Li, S. Cai, L. Tian, K. Chen, J. Wang, J. Hu, Y. Sun, X. Li, A. Ertel, R.G. Pestell, EYA1 phosphatase function is essential to drive breast cancer cell proliferation through cyclin D1, *Cancer research*, 73 (2013) 4488-4499.
- [5] E. Tadjuidje, R.S. Hegde, The Eyes Absent proteins in development and disease, *Cellular and molecular life sciences : CMLS*, 70 (2013) 1897-1913.
- [6] M. Weinfeld, R.S. Mani, I. Abdou, R.D. Aceytuno, J.N. Glover, Tidying up loose ends: the role of polynucleotide kinase/phosphatase in DNA strand break repair, *Trends in biochemical sciences*, 36 (2011) 262-271.
- [7] G.K. Freschauf, F. Karimi-Busheri, A. Ulaczyk-Lesanko, T.R. Mereniuk, A. Ahrens, J.M. Koshy, A. Rasouli-Nia, P. Pasarj, C.F. Holmes, F. Rininsland, D.G. Hall, M. Weinfeld, Identification of a small molecule inhibitor of the human DNA repair enzyme polynucleotide kinase/phosphatase, *Cancer research*, 69 (2009) 7739-7746.
- [8] A.B. Krueger, S.J. Dehdashti, N. Southall, J.J. Marugan, M. Ferrer, X. Li, H.L. Ford, W. Zheng, R. Zhao, Identification of a selective small-molecule inhibitor series targeting the eyes absent 2 (Eya2) phosphatase activity, *Journal of biomolecular screening*, 18 (2013) 85-96.
- [9] J.E. Hawkinson, M. Acosta-Burrue, P.L. Wood, The metabotropic glutamate receptor antagonist L-2-amino-3-phosphonopropionic acid inhibits phosphoserine phosphatase, *European journal of pharmacology*, 307 (1996) 219-225.
- [10] E. Tadjuidje, T.S. Wang, R.N. Pandey, S. Sumanas, R.A. Lang, R.S. Hegde, The EYA tyrosine phosphatase activity is pro-angiogenic and is inhibited by benzbromarone, *PLoS one*, 7 (2012) e34806.
- [11] H. Park, S.K. Jung, K.R. Yu, J.H. Kim, Y.S. Kim, J.H. Ko, B.C. Park, S.J. Kim, Structure-based virtual screening approach to the discovery of novel inhibitors of eyes absent 2 phosphatase with various metal chelating moieties, *Chemical biology & drug design*, 78 (2011) 642-650.
- [12] M. Zhang, E.J. Cho, G. Burstein, D. Siegel, Y. Zhang, Selective inactivation of a human neuronal silencing phosphatase by a small molecule inhibitor, *ACS chemical biology*, 6 (2011) 511-519.
- [13] K.N. Allen, D. Dunaway-Mariano, Markers of fitness in a successful enzyme superfamily, *Current opinion in structural biology*, 19 (2009) 658-665.
- [14] C. Kestler, G. Knobloch, I. Tessmer, E. Jeanclous, H. Schindelin, A. Gohla, Chronophin dimerization is required for proper positioning of its substrate specificity loop, *The Journal of biological chemistry*, 289 (2014) 3094-3103.
- [15] A. Gohla, J. Birkenfeld, G.M. Bokoch, Chronophin, a novel HAD-type serine protein phosphatase, regulates cofilin-dependent actin dynamics, *Nature cell biology*, 7 (2005) 21-29.
- [16] M.L. Fonda, Purification and characterization of vitamin B6-phosphate phosphatase from human erythrocytes, *The Journal of biological chemistry*, 267 (1992) 15978-15983.

- [17] R. Percudani, A. Peracchi, A genomic overview of pyridoxal-phosphate-dependent enzymes, *EMBO reports*, 4 (2003) 850-854.
- [18] A.C. Eliot, J.F. Kirsch, Pyridoxal phosphate enzymes: mechanistic, structural, and evolutionary considerations, *Annual review of biochemistry*, 73 (2004) 383-415.
- [19] H. Zuo, P.M. Ueland, S.J. Eussen, G.S. Tell, S.E. Vollset, O. Nygard, O. Midttun, K. Meyer, A. Ulvik, Markers of vitamin B6 status and metabolism as predictors of incident cancer: The Hordaland Health Study, *International journal of cancer. Journal international du cancer*, (2014).
- [20] M. Johansson, C. Relton, P.M. Ueland, S.E. Vollset, O. Midttun, O. Nygard, N. Slimani, P. Boffetta, M. Jenab, F. Clavel-Chapelon, M.C. Boutron-Ruault, G. Fagherazzi, R. Kaaks, S. Rohrmann, H. Boeing, C. Weikert, H.B. Bueno-de-Mesquita, M.M. Ros, C.H. van Gils, P.H. Peeters, A. Agudo, A. Barricarte, C. Navarro, L. Rodriguez, M.J. Sanchez, N. Larranaga, K.T. Khaw, N. Wareham, N.E. Allen, F. Crowe, V. Gallo, T. Norat, V. Krogh, G. Masala, S. Panico, C. Sacerdote, R. Tumino, A. Trichopoulou, P. Lagiou, D. Trichopoulos, T. Rasmuson, G. Hallmans, E. Riboli, P. Vineis, P. Brennan, Serum B vitamin levels and risk of lung cancer, *Jama*, 303 (2010) 2377-2385.
- [21] L. Galluzzi, I. Vitale, L. Senovilla, K.A. Olaussen, G. Pinna, T. Eisenberg, A. Goubar, I. Martins, J. Michels, G. Kratassiouk, D. Carmona-Gutierrez, M. Scoazec, E. Vacchelli, F. Schlemmer, O. Kepp, S. Shen, M. Tailler, M. Niso-Santano, E. Morselli, A. Criollo, S. Adjemian, M. Jemaa, K. Chaba, C. Pailleret, M. Michaud, F. Pietrocola, N. Tajeddine, T. de La Motte Rouge, N. Araujo, N. Morozova, T. Robert, H. Ripoche, F. Commo, B. Besse, P. Validire, P. Fouret, A. Robin, N. Dorvault, P. Girard, S. Gouy, P. Pautier, N. Jagemann, A.C. Nickel, S. Marsili, C. Paccard, N. Servant, P. Hupe, C. Behrens, P. Behnam-Motlagh, K. Kohno, I. Cremer, D. Damotte, M. Alifano, O. Midttun, P.M. Ueland, V. Lazar, P. Dessen, H. Zischka, E. Chatelut, M. Castedo, F. Madeo, E. Barillot, J. Thomale, Wistuba, II, C. Sautes-Fridman, L. Zitvogel, J.C. Soria, A. Harel-Bellan, G. Kroemer, Prognostic impact of vitamin B6 metabolism in lung cancer, *Cell reports*, 2 (2012) 257-269.
- [22] L. Galluzzi, E. Vacchelli, J. Michels, P. Garcia, O. Kepp, L. Senovilla, I. Vitale, G. Kroemer, Effects of vitamin B6 metabolism on oncogenesis, tumor progression and therapeutic responses, *Oncogene*, 32 (2013) 4995-5004.
- [23] J. Hou, J. Aerts, B. den Hamer, W. van Ijcken, M. den Bakker, P. Riegman, C. van der Leest, P. van der Spek, J.A. Foekens, H.C. Hoogsteden, F. Grosveld, S. Philipsen, Gene expression-based classification of non-small cell lung carcinomas and survival prediction, *PloS one*, 5 (2010) e10312.
- [24] T.L. Hullar, Pyridoxal phosphate. I. Phosphonic acid analogs of pyridoxal phosphate. Synthesis via Wittig reactions and enzymic evaluation, *Journal of medicinal chemistry*, 12 (1969) 58-63.
- [25] R.F. Struck, Y.F. Shealy, J.A. Montgomery, Vitamin B6 analogs. 4. 4-Desoxyisopyridoxal and the phosphonic acid analog of 4-desoxypyridoxine phosphate, *Journal of medicinal chemistry*, 14 (1971) 568-571.
- [26] R.J. Kubiak, K.S. Bruzik, Comprehensive and uniform synthesis of all naturally occurring phosphorylated phosphatidylinositols, *The Journal of organic chemistry*, 68 (2003) 960-968.
- [27] G.J. Gao, M.L. Fonda, Kinetic analysis and chemical modification of vitamin B6 phosphatase from human erythrocytes, *The Journal of biological chemistry*, 269 (1994) 7163-7168.
- [28] T.G. Battye, L. Kontogiannis, O. Johnson, H.R. Powell, A.G. Leslie, iMOSFLM: a new graphical interface for diffraction-image processing with MOSFLM, *Acta crystallographica. Section D, Biological crystallography*, 67 (2011) 271-281.
- [29] P. Evans, Scaling and assessment of data quality, *Acta crystallographica. Section D, Biological crystallography*, 62 (2006) 72-82.
- [30] A.J. McCoy, R.W. Grosse-Kunstleve, P.D. Adams, M.D. Winn, L.C. Storoni, R.J. Read, Phaser crystallographic software, *Journal of applied crystallography*, 40 (2007) 658-674.
- [31] N.W. Moriarty, R.W. Grosse-Kunstleve, P.D. Adams, electronic Ligand Builder and Optimization Workbench (eLBOW): a tool for ligand coordinate and restraint generation, *Acta crystallographica. Section D, Biological crystallography*, 65 (2009) 1074-1080.
- [32] P.D. Adams, P.V. Afonine, G. Bunkoczi, V.B. Chen, I.W. Davis, N. Echols, J.J. Headd, L.W. Hung, G.J. Kapral, R.W. Grosse-Kunstleve, A.J. McCoy, N.W. Moriarty, R. Oeffner, R.J. Read, D.C. Richardson, J.S. Richardson, T.C. Terwilliger, P.H. Zwart, PHENIX: a comprehensive Python-based system for

macromolecular structure solution, *Acta crystallographica. Section D, Biological crystallography*, 66 (2010) 213-221.

[33] P.D. Adams, P.V. Afonine, G. Bunkoczi, V.B. Chen, N. Echols, J.J. Headd, L.W. Hung, S. Jain, G.J. Kapral, R.W. Grosse Kunstleve, A.J. McCoy, N.W. Moriarty, R.D. Oeffner, R.J. Read, D.C. Richardson, J.S. Richardson, T.C. Terwilliger, P.H. Zwart, The Phenix software for automated determination of macromolecular structures, *Methods*, 55 (2011) 94-106.

[34] P.V. Afonine, R.W. Grosse-Kunstleve, P.D. Adams, V.Y. Lunin, A. Urzhumtsev, On macromolecular refinement at subatomic resolution with interatomic scatterers, *Acta crystallographica. Section D, Biological crystallography*, 63 (2007) 1194-1197.

[35] V.B. Chen, W.B. Arendall, 3rd, J.J. Headd, D.A. Keedy, R.M. Immormino, G.J. Kapral, L.W. Murray, J.S. Richardson, D.C. Richardson, MolProbity: all-atom structure validation for macromolecular crystallography, *Acta crystallographica. Section D, Biological crystallography*, 66 (2010) 12-21.

ACCEPTED MANUSCRIPT

Fig. 1

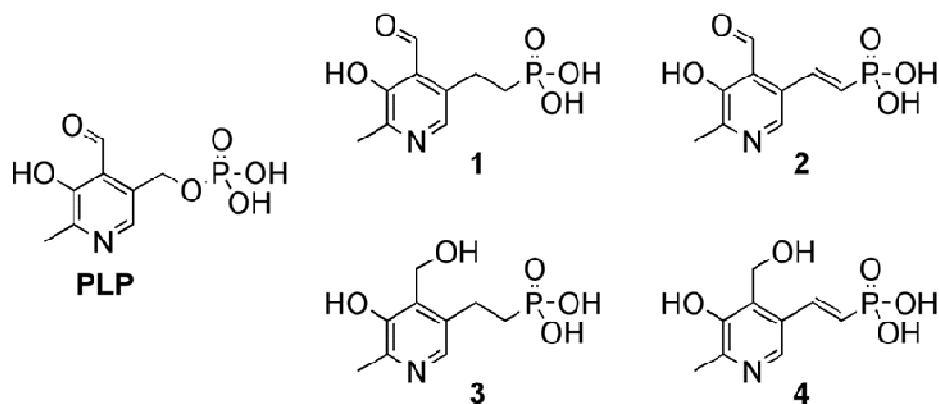
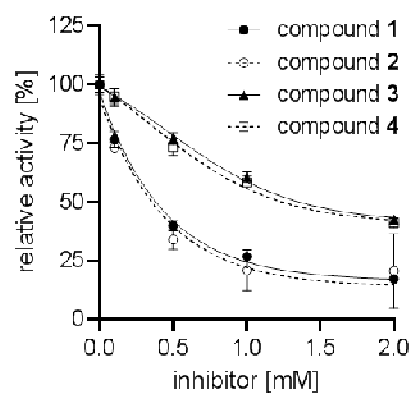
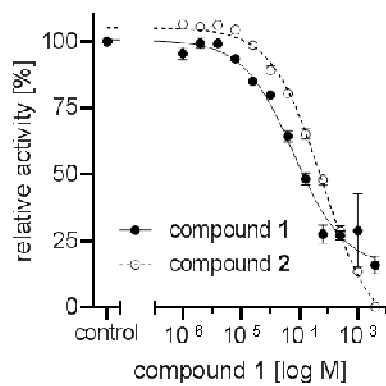


Fig. 2

A

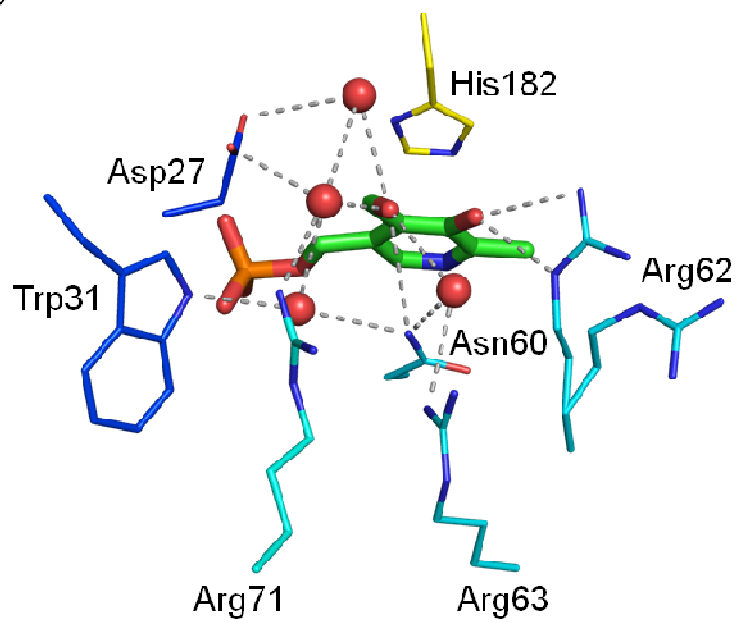


B



ACCEPTED MANUSCRIPT

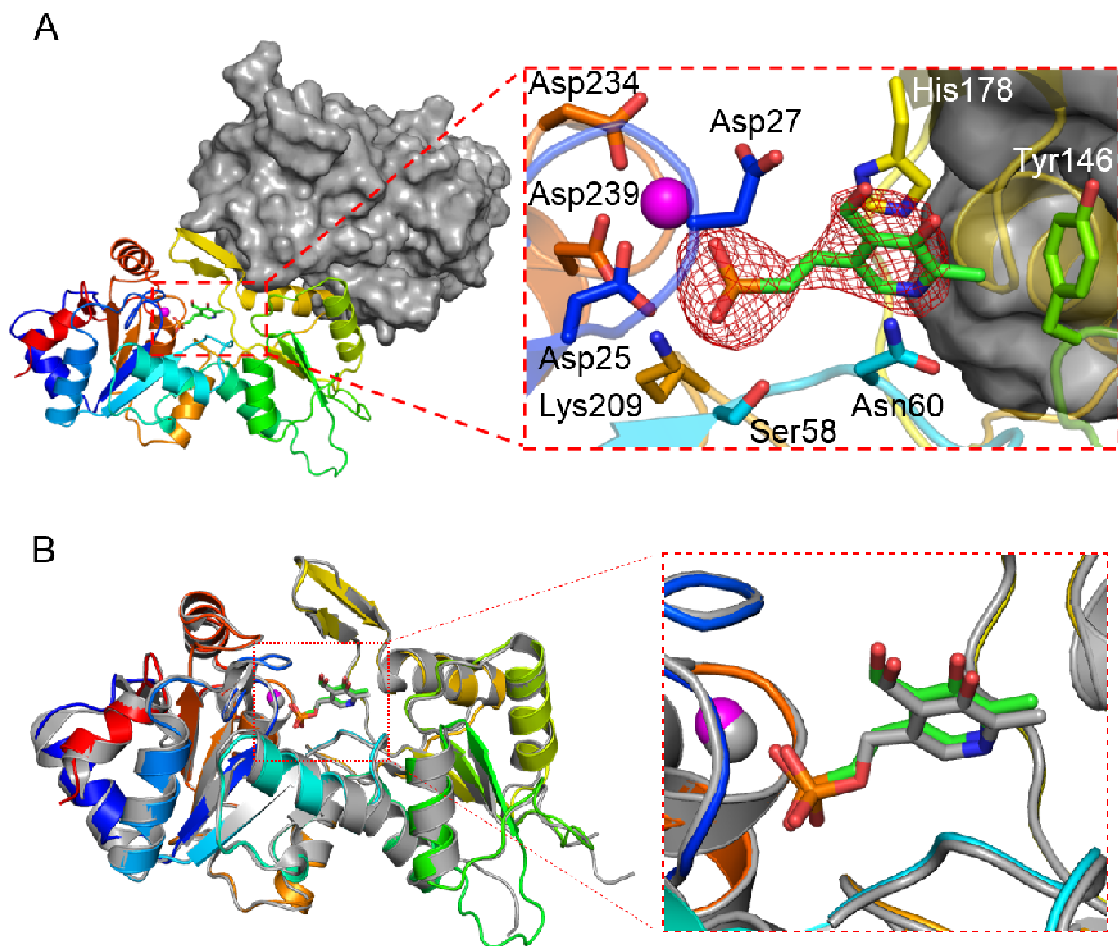
Fig. 3



ACCEPTED M

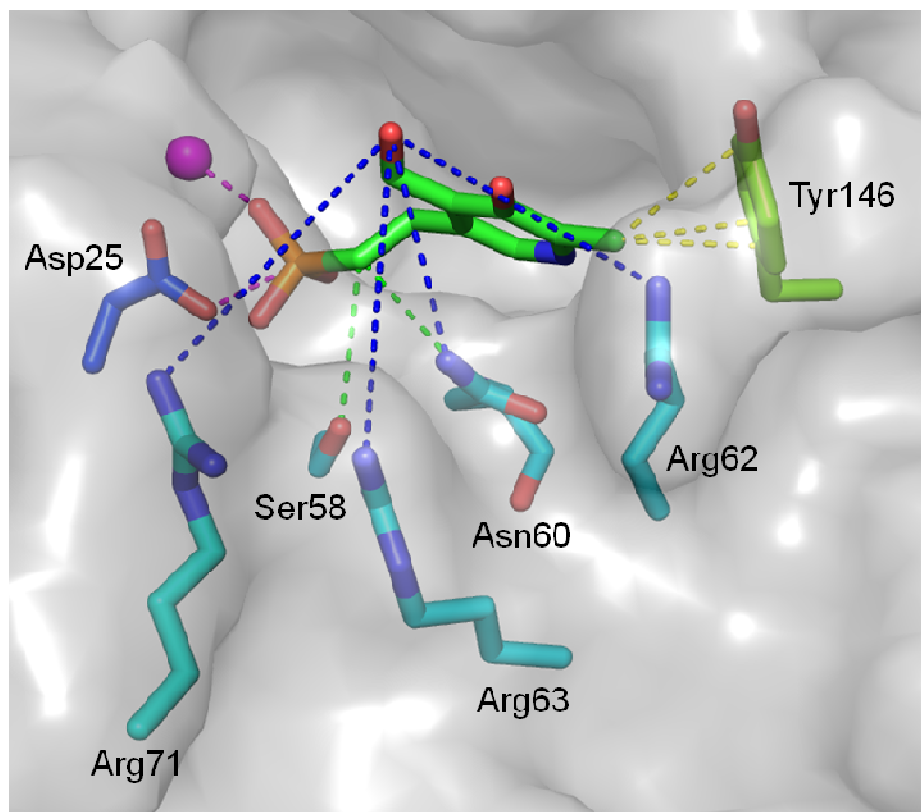
SCRIPT

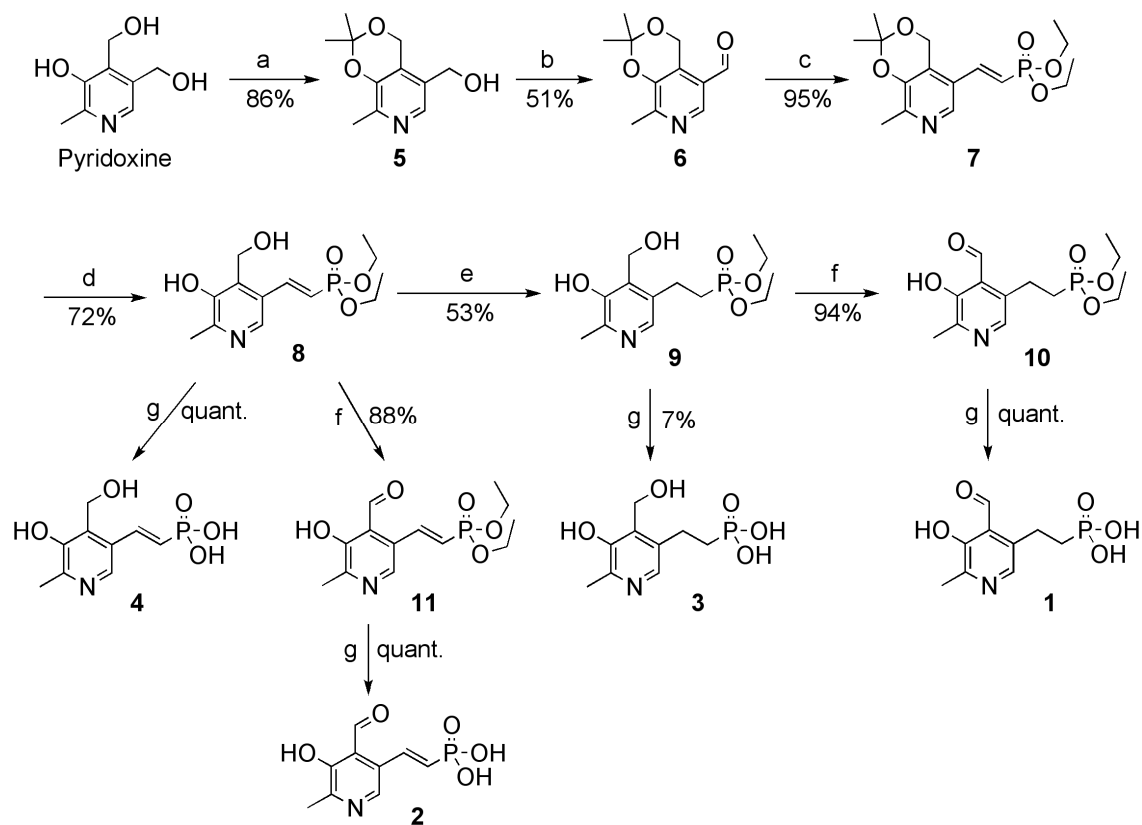
Fig. 4



ACCEPT

Fig. 5





## Graphical abstract

